CrossMark

Studies of thermo-electric power and dielectric modulus of polypyrrole/zirconium oxide-molybdenum trioxide (PZM) composites

R. Harshitha[1] · V. B. Aaditya[2] · B. M. Bharathesh[3] · B. V. Chaluvaraju[1] · U. P. Raghavendra[1] · M. V. Murugendrappa[4,5]

Abstract

Zirconium oxide-molybdenum trioxide doped polypyrrole composites have been synthesized in the presence of ammonium persulphate (oxidizing agent), with different 15, 30, 45 and 60 wt% of zirconium oxide-molybdenum trioxide (ZM) in pyrrole, by the chemical polymerization (oxidation) process. The polypyrrole/zirconium oxide-molybdenum trioxide (PZM) composites have exhibited crystalline nature, which has been confirmed by powder X-ray diffraction patterns. The Fourier transform infrared graphs show that the stretching frequencies of the composites have shifted towards the lower frequency side. The scanning electron microscopy micrographs indicate that the composites are of spherical nature and form elongated chains; an increase in the particles size when compared with polypyrrole and ZM particles is also observed. Thermo electric power and transport properties studies reveal that there is an interaction between polypyrrole and the ZM particles and the weight percents of the ZM particles have an influence on the properties of the pure polypyrrole. Studies shown that, the PZM composites are good materials in conductivity, dielectric properties, micro power generator, thermo cooling, as semiconductors as well as may be in humidity, gas and thermal sensor.

1 Introduction

Developments in science and technology have revealed fresh applications possibilities for conducting polymers and their derivatives. Intrinsically conducting polymers [1–12], by virtue of their light weight and greater ease of fabrication, have replaced and are proceeding to replace metals in several areas of applications. Several conducting polymers have already been prepared for a wide range of applications [13], from rechargeable batteries to microwave absorption [14–16].

✉ B. V. Chaluvaraju
chaluvaraju@bit-bangalore.edu.in; bvcgowda@gmail.com

1   Department of Physics, Bangalore Institute of Technology, Bengaluru, Karnataka 560004, India

2   Chalmer's University of Technology, Goteberg, Sweden

3   KTH Royal Institute of Technology, Stockholm, Sweden

4   Department of Physics, BMS College of Engineering, Bengaluru, Karnataka 560019, India

5   Center of Excellence in Advanced Materials Research, BMS College of Engineering, Bengaluru, Karnataka 560019, India

Polypyrrole [17] can be synthesized either chemically [18] or by the electro-chemically polymerization technique. Synthesized polypyrrole has a better electrical conductivity [19] rendering its versatility in applications like batteries, electronic devices, functional electrodes, electro-chromic devices, optical switching devices, sensors [20] etc. Conducting polymer based composites have become increasingly important for technical applications such as humidity and gas sensors [21–23] as well as thermo electric power, which might make it an important player in the field of power generation i.e. micro power generators and coolers.

In this article, the authors have studied the thermo-electrical power, dielectric electrical modulus and other transport properties of the zirconium oxide-molybdenum trioxide doped polypyrrole (PZM) composites. These were prepared with the help of the chemical polymerization technique.

The main applications of ZrO_2 are Precision ball valve balls and seats, high density ball and pebble mill grinding media, rollers and guides for metal tube forming, thread and wire guides, hot metal extrusion dies, deep well down-hole valves and seats, powder compacting dies, marine pump seals and shaft guides, oxygen sensors, high temperature induction furnace susceptors, fuel cell membranes, electric

furnace heaters over 2000 °C in oxidizing atmospheres, etc [24–26].

The main applications of MoO_3 are as an adhesive between enamels and metals, as an additive to steel and corrosion-resistant alloys, as a co-catalyst, as a component in electrochemical devices and displays. Molybdenum trioxide has also been suggested as apotential anti-microbial agent, e.g., in polymers. In contact with water, it forms H^+ ions that can kill bacteria effectively [27–30].

The d.c. conductivity of the synthesized composites were determined to be better than some synthesized conducting polymer based composites such as polypyrrole/ZrO_2 composites (0.2 m S/cm) [24–26], polypyrrole/MoO_3 composites (298 µ S/cm) [27–30], polypyrrole/Ta_2O_5 composites (260 µ S/cm) [31], polyamide-66/multi-walled carbon nanotube composites (10^{-5} S/cm) [32], polypyrrole-polymannuronate nanocomposites (11.95×10^{-4} S/cm) [33], polypyrrole/sodium metavanadate composites (0.167 m S/cm) [34], polypyrrole/zinc tungstate composites (0.256 m S/cm), polypyrrole/strontium arsenate composites (0.24 m S/cm), etc. (the last two composites were prepared in our laboratory).

Thermo-electricity is the science and technology associated with thermo-electric converters, i.e. the generation of electrical power [35, 36]. Thermo-electric generators have been utilized to cater to electrical power requirements for medical, military, space, automobile and industrial applications and are also used in portable refrigerators, water coolers, car air conditioners, thermal energy sensors and for stabilizing ink temperature in printers and copiers. Further, interest in thermo-electrics has enhanced with the advent of several semiconductor thermo elements [37].

Direct conversion of heat into electricity through advanced thermoelectric (TE) materials is one of the most attractive solutions to depleting conventional energy sources and several related environmental factors faced by humanity [38]. Energy demands have been growing due to escalating human needs as well as concerns over depletion of the fossil fuel resources and climatic changes. These have led to a concerted effort to develop sustainable technologies for efficient use, conversion and recovery of energy. One such technology is the use of TE materials to directly convert heat into electricity based on the Seebeck effect [39–45]. It is known, that one can also apply electrical voltage to TE materials to induce cooling, through the Peltier effect. Detailed principles of TE conversions have also been described in books and research papers [33–36]. This technology has a number of distinct advantages. They are (1). TE conversion is reliable and operates in silence when compared with other energy conversion technologies, as it works without mechanical movement, (2). TE devices are simple, compact and safe, (3). it is an environmentally friendly, green technology, because no heat and no gaseous or chemical waste are produced during operation and (4). it can be widely used in places where other energy conversion technologies are unavailable i.e. remote outer space [39, 40].

Thermo-electric properties for a material depend upon the charge concentration. Metals are poor TE materials which have low Seebeck coefficient, because they have a large electronic contribution to the thermal conductivity. Insulators on the other hand have high Seebeck coefficient and a small electronic contribution. Thus, the best TE materials are those between metals and insulators. Hence, conducting polymers based composites are more promising TE materials since they possess stronger stability than conducting poymers. We have found work on some polymer TE materials in our literature survey [46–48].

2 Experimental details

2.1 Synthesis

2.1.1 Synthesis of the pure polypyrrole

0.06 M ammonium per sulphate (oxidative agent) [49] was prepared using 13.69 g of ammonium persulphate weighed (up to second decimal) by with a digital balance and transferred to a conical flask (Borosil: 250 ml). 100 ml distilled water was measured by using a measuring jar (Borosil: 100 ml) and transferred to the same conical flask. The conical flask was shaken well several times to obtain the required 0.06 M ammonium persulphate solution. The above solution was filled in a burette attached to a laboratory stand for use in further processes.

A. R. grade (Spectro Chem Pvt. Ltd., Bengaluru Division, Bengaluru, India) pyrrole purification has been done by the distillation technique. 0.3 M [50] pyrrole monomer i.e. 10.4 ml was measured by using a burette and transferred into a beaker (Borosil: 1000 ml). 500 ml distilled water was measured by using a measuring jar and transferred into the same beaker. The beaker was well shaken to obtain a properly mixed pyrrole monomer solution. The beaker was kept on a plastic tray and ice-flakes (obtained by a continuous automatic ice-maker) were placed around the beaker. The temperature was maintained between 0° and 5 °C [51]. Then the tray was placed on a magnetic stirrer and a magnetic bead was dropped into the beaker, which helped the solution to rotate either in the clockwise or the anticlockwise direction, by means of a selection switch. The selected RPM (rotation per minute) of the magnetic bead ranged from 1500 to 2200.

Ammonium persulphate solution was now added [52] drop wise to the pyrrole solution. Chemical reaction i.e. polymerization started and the pyrrole solution gradually

turned black, due to the polymerization. This process was continued for 5 h [53] until a precipitate formed.

A filter paper was appropriately cut to snugly fit into the Buckner funnel. The polypyrrole precipitate solution was slowly poured into the Buckner funnel, which was kept in a side neck conical flask. Water was absorbed from the precipitate by using a vacuum pump. The precipitate thus obtained was transferred to a petri dish and kept in a hot air oven which was maintained at a maximum temperature of 100 °C. The precipitate was dried for approximately 8–10 h and later ground using an agate mortar. The ground powder was poured into a crucible and kept in the muffle furnace to complete the drying process. The dehumidification of the black polypyrrole precipitate was continued for about 4–6 h in the muffle furnace at a maximum temperature of 100 °C. The completely dried black polypyrrole powder was then removed from the muffle furnace and ground into a finer powder. The weight of the black polypyrrole powder thus obtained was 3.17 g. It was labeled as sample 1 of the polypyrrole [54–57].

Similarly, the above procedure was employed to get the black polypyrrole powder which was labeled as sample 2 which weighed 3.23 g. Average weight of both samples of the pure polypyrrole powders was taken as the weight of the synthesized polypyrrole sample which was 3.20 g. This was done for experimental optimization of the polypyrrole.

2.1.2 Synthesis of the polypyrrole/zirconium oxide-molybdenum trioxide (PZM) composites

0.48 g (15 wt%) of zirconium oxide-molybdenum trioxide (ZM) (zirconium oxide and molybdenum trioxide, Sisco Research Lab Ltd., Bengaluru Division, Bengaluru, India) was added to the 0.3 M pyrrole solution and mixed thoroughly. Further, 0.06 M APS was continuously added dropwise, with the help of a burette, to the above solution, to get a zirconium oxide-molybdenum trioxide doped polypyrrole (PZM) 15% nano composite [55]. Similarly, for 30, 45 and 60 wt%, 0.96, 1.44 and 1.92 g of PZM powder was taken and the above procedure repeated to get the nanocomposites. The yields of the nanocomposites were 4.33, 4.68, 4.98 and 7.05 g respectively.

The real content of zirconium oxide-molybdenum trioxide (ZM) in PPy matrix was determined as follows:

Sample (10 wt%) = (yield of the sample × 10)/100 = … g

For example: MoO_3 (10 wt%) = (3.2 × 10)/100 = 0.32 g

ZrO_2 (15 wt%) = (3.2 × 15)/100 = 0.48 + MoO_3 (15 wt%) = (3.2 × 15)/100 = 0.48

ZrO_2 (7.5 wt%) = (3.2 × 15)/100 = 0.24 + MoO_3 (7.5 wt%) = (3.2 × 15)/100 = 0.24

ZrO_2–MoO_3 (15 wt%) = (3.2 × 15)/100 = 0.24 + 0.24 = 0.48 g

ZrO_2 (30 wt%) = (3.2 × 30)/100 = 0.96 + MoO_3 (30 wt%) = (3.2 × 30)/100 = 0.96

ZrO2 (15 wt%) = (3.2 × 15)/100 = 0.48 + MoO3 (15 wt%) = (3.2 × 15)/100 = 0.48

ZrO_2–MoO_3 (30 wt%) = (3.2 × 15)/100 = 0.48 + 0.48 = 0.96 g

ZrO_2 (45 wt%) = (3.2 × 45)/100 = 1.44 + MoO_3 (45 wt%) = (3.2 × 45)/100 = 1.44

ZrO_2 (22.5 wt%) = (3.2 × 22.5)/100 = 0.72 + MoO_3 (22.5 wt%) = (3.2 × 22.5)/100 = 0.72

ZrO_2–MoO_3 (45 wt%) = (3.2 × 45)/100 = 0.72 + 0.72 = 1.44 g

ZrO_2 (60 wt%) = (3.2 × 60)/100 = 1.92 + MoO_3 (60 wt%) = (3.2 × 60)/100 = 1.92

ZrO_2 (30 wt%) = (3.2 × 30)/100 = 0.96 + MoO_3 (30 wt%) = (3.2 × 30)/100 = 0.96

ZrO_2–MoO_3 (60 wt%) = (3.2 × 60)/100 = 0.96 + 0.96 = 1.92 g

The pure polypyrrole and PZM nano composites powder were compressed into pellets of 1–3 mm thickness and 1 cm diameter by applying 10–12 tons pressure, using a hydraulic press (Shimazdu, Tokyo, Japan) [22]. Silver paste was applied to both sides of the pellets, of the synthesized composites, for the d.c. conductivity and thermo e. m. f. measurements. d.c. conductivity (SES Instruments Private Limited, Bengaluru Division, Bengaluru, India) for the synthesized composites was measured in the temperature range from 200 to 50 °C [27–30] with suitable constant voltages (1.2 and 2 V). The temperatures of cold and hot junctions and corresponding thermo e. m. f. were measured at different temperatures in the temperature range from 323 to 473 K with the help of a thermo-electric power device (SES Instruments Pvt. Ltd., Bengaluru, India). The 6500B series of Precision Impedance Analyzers (Wayne Kerr Electronics Pvt. Ltd., Bengaluru Division, Bengaluru, India) was used for the measurement of the a.c. conductivity, dielectric relative permittivity, dielectric loss and tangent loss parameters, in the frequency range from 20 Hz to 1 MHz, at room temperature for the composites.

2.2 Characterization

The FTIR spectra of polypyrrole, PZM composites and ZM have been recorded on a FTIR (Perkin Elmer, Bengaluru Division, Bengaluru, India) spectrometer, in a medium of potassium bromide, at room temperature. The XRD patterns of the samples was recorded on a X-ray Diffractometer (Bruker AXS D8 Advance, Bengaluru Division, Bengaluru, India), using Cu Kα radiation (λ = 1.5418 Å), in the 2θ range of 5°–90°. SEM micrographs were obtained using a Scanning Electron Microscope (Jeol 6390 LV, Bengaluru Division, Bengaluru, India).

3 Results and discussion

3.1 SEM analysis

Figure 1a–d are the SEM micrographs of the pure polypyrrole, PZM (15 and 45%) composites and ZM respectively. It is clearly seen from the SEM micrograph of polypyrrole, that it has clusters of spherical shaped particles as well as elongated chain patterns of the polypyrrole particles. The granular morphology of the polypyrrole particle structures was measured. The SEM micrographs of the composites are indicative of a spherical nature of polymer occurring as clusters in the composites. The ZM particles are embedded in the PPy chain, presumably because of weak inter-particle interactions. The SEM micrograph of ZM shows that the ZM particles exhibit crystalline structures [33, 56–63]. Different sample particle sizes are visible in the figures. The particle sizes of the composites have increased when compared with polypyrrole and ZM particles.

3.2 FTIR analysis

The FTIR spectra of ZM, PZM composites and pure PPy are shown in Fig. 2. When PZM composites were compared with polypyrrole and ZM, the stretching frequencies were
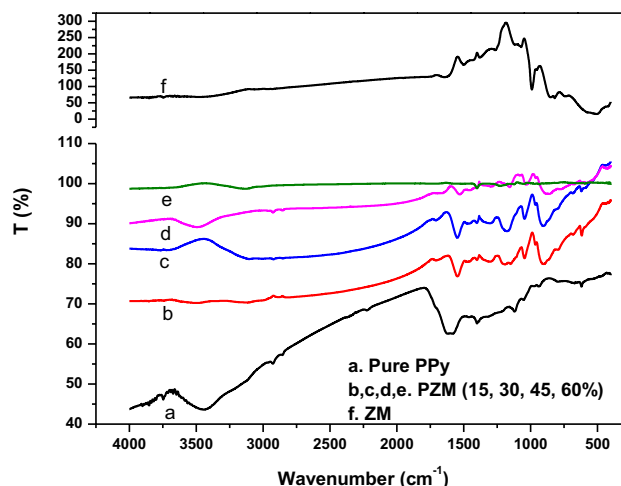
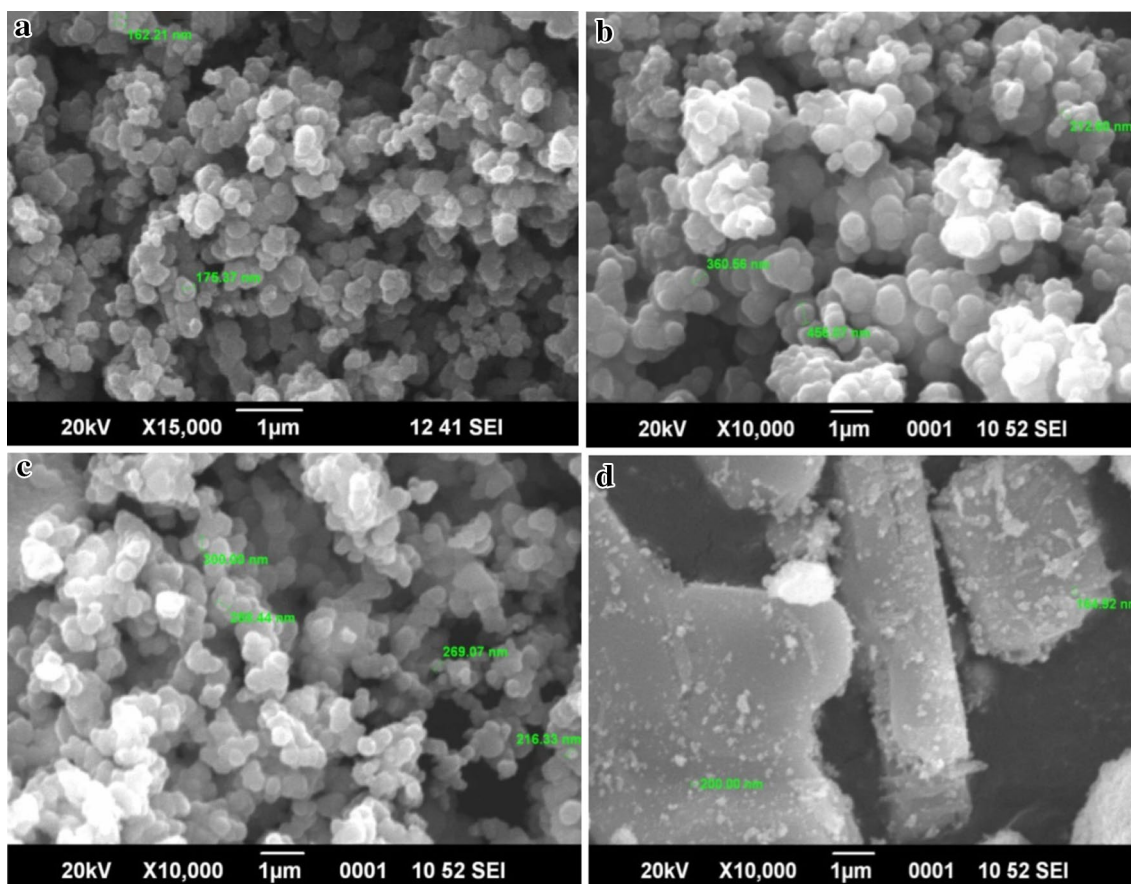**Fig. 2** FTIR graphs of polypyrrole, PZM nano composites and ZM

Fig. 1 a–d SEM micrographs of the pure polypyrrole, PZM (15 and 45%) composites and ZM

found to have shifted towards the lower frequency side. It may be attributed to the existence of N–H bending deformation, C=N stretching, C–H bending deformation and C–N stretching frequencies. This indicates that there was a homogeneous distribution of ZM particles in the chains of polymer, due to the Van der Walls interaction between the ZM particles and chains of polymer [63–76].

3.3 XRD analysis

Figure 3a represents the X-ray diffraction pattern of the pure PPy, which has a broad peak at about $2\theta = 25°$, which is a characteristic peak of amorphous polypyrrole. The XRD patterns (Fig. 3b–e) of the PZM composites suggest that they exhibit a high degree of crystallinity. Figure 3f represents
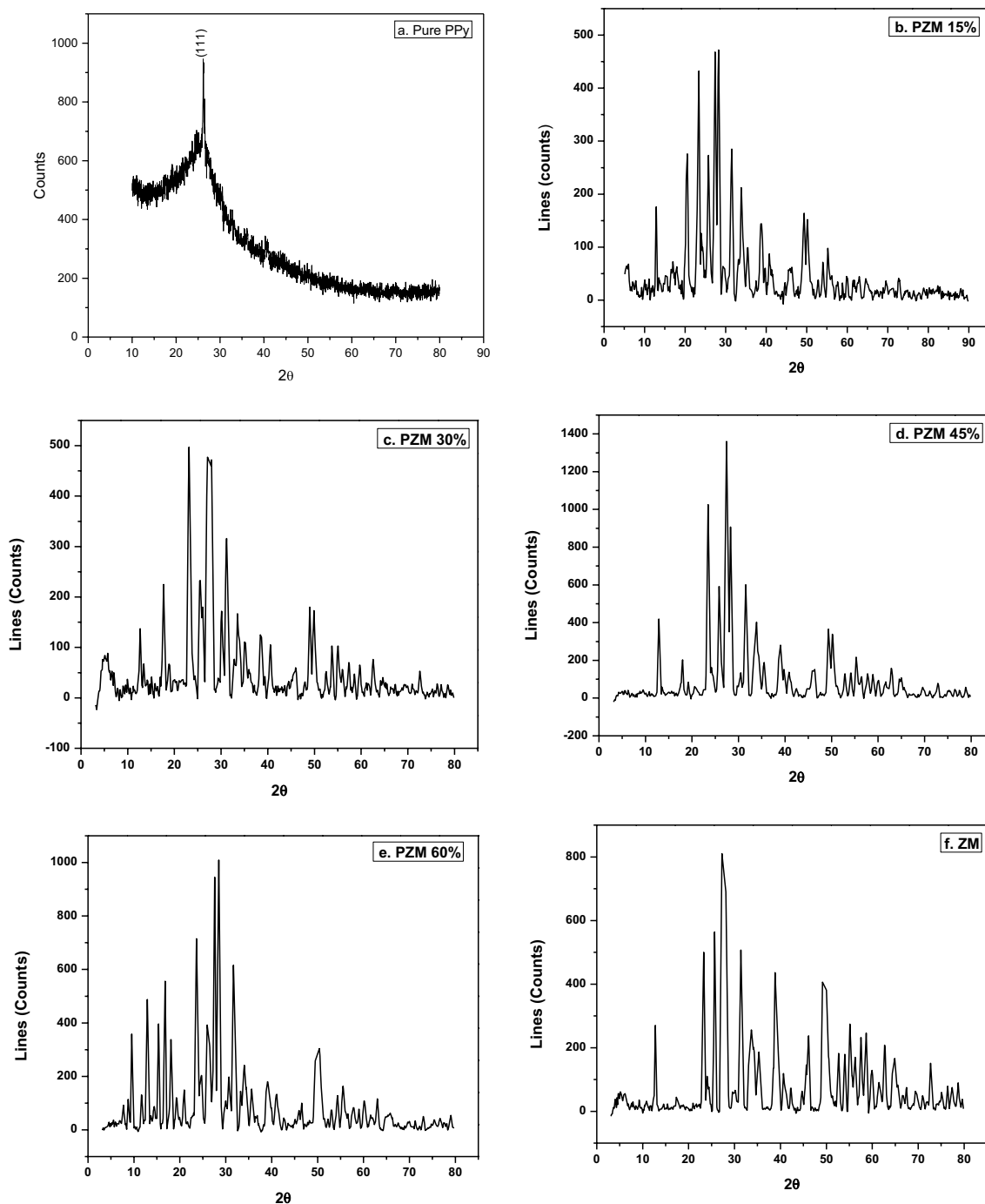

**Fig. 3 a–f** XRD patterns of polypyrrole, PZM nanocomposites and ZM

the XRD pattern of ZM also revealing the crystalline nature [77–83].

Mixture of amorphous polypyrrole and crystalline ZM yields the PZM composites with high degree of crystallinity.

3.4 d.c. conductivity study

The current remains constant till a temperature of 150 °C and then increases exponentially till 200 °C (Fig. 4a). The d.c. conductivity also displays a similar behavior (Fig. 4b). The conductivity values recorded for the composites at 200 °C are 7.56, 7.63, 7.32 and 5.61 (m S/cm) respectively. The nanocomposites (except 60 wt%) have approximately equal conductivity. The nano-composite (30 wt%) has the highest conductivity, due to the extended chain length of the pure polypyrrole, which facilitates the hopping of charge carriers and may also be promoting a larger number of charge carriers to hop between favorable localized sites. The decrease in the conductivity for the PZM (60 wt%) nanocomposite may be due to the extended chain length of polypyrrole, which now doesn't facilitate the hopping of charge carriers when the concentration of ZM is high and may additionally be attributed to the trapping of charge carriers. Charge trapping in polypyrrole and its composites is an universal feature [27–31].
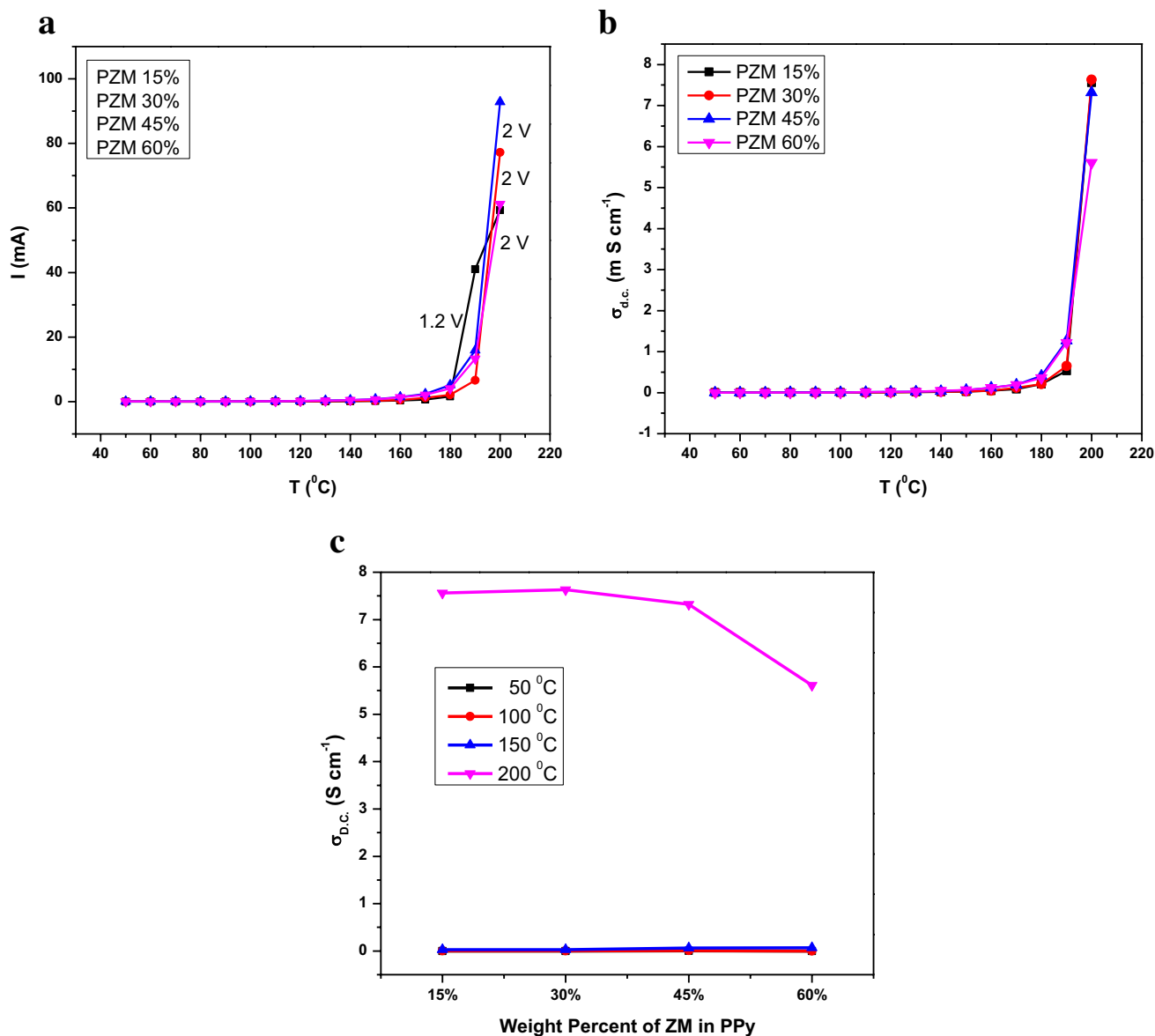
Fig. 4 a Current vs. temperature for the PZM composites. **b** d.c. conductivity versus temperature for PZM nanocomposites. **c** d.c. conductivity vs. weight percent for the PZM nanocomposites

Conductivity increases (Fig. 4c) for all the composites at 200 °C. The conductivity is maximum at 30 wt% of ZM in the pure polypyrrole, whereas it decreases for the other composites. This weight percent is the percolation threshold for these composites. Hence, the composites obey percolation theory [27–31].

3.5 Thermo-electric power study

Theory: thermo-electric (TE) technology possesses several merits and has been known for more than one century.The conversion efficiency strongly depends on the figure of merit (ZT) of the TE material [44], as given by Eq. (1),

$$\eta = \eta_c \left[\sqrt{1 + \sqrt{ZT}} - 1 \right] / \left[\left(\sqrt{1 + \sqrt{ZT}} \right) + (T_c/T_h) \right] \quad (1)$$

where η is the conversion efficiency of heat to electricity, T_c and T_h are the temperatures of cold and hot sides of a TE generator respectively, η_c represents the Carnot efficiency and can be expressed as $\eta_c = 1 - T_c/T_h$.

Figure of merit (ZT) [44], is given by Eq. (2),

$$ZT = S^2 \sigma_{d.c.} T/\kappa \quad (2)$$

where S is the Seebeck coefficient, $\sigma_{d.c.}$ is the d.c. electrical conductivity, κ is the thermal conductivity, T is absolute temperature and $S^2 \sigma_{d.c.}$ is the thermo power factor.

A temperature gradient between the two ends of a sample gives rise to an e. m. f. known as thermo e. m. f. (V_s) or See-beck voltage. If a sample is maintained at two different temperatures, a See-beck voltage can manifest due to the fact that the majority carriers diffuse from a surface having high temperature (T_2) to a surface with relatively lower temperature (T_1). It has also been observed that, the generated thermo e. m. f. is proportional to the temperature difference ($\Delta T = T_2 - T_1$) between two surfaces of the sample and given by the relation,

$$S = V_s / (T_2 - T_1) = V_s / \Delta T$$

where S is thermo-electric power.

Thermo-electric power is of great interest in understanding the transport properties, due to its extreme sensitivity to the change of electronic structure, at the Fermi energy. As the lattice thermal conductivity dominates over the electronic contribution for most materials used for room temperature applications, the single electronic parameter that describes the efficiency of a thermoelectric cooler or a power generator is the thermoelectric power factor. In conventional metals or semiconductors, increasing the electrical conductivity decreases the Seebeck coefficient, which is mainly due to the three dimensional nature of the electronic density of states [84].

Experimental Procedure: The experimental device to determine the thermo e. m. f. of the composites consists of a point contact probe which acts as a hot junction and a base which acts as a cold junction. A sample is kept between the two junctions. Pellets of 1 cm diameter and 1–3 mm thickness have been used in the present study. The hot and cold probes were connected to a digital milli-voltmeter for the measurement of thermo e. m. f. The temperature of the hot junction is raised by using a dimmerstat till it attains a temperature of 200 °C. The hot junction temperature was then decreased from 200 to 50 °C in steps of 10 °C and the temperatures of the cold and hot junctions as well as the thermo e. m. f. recorded [84].

It was observed that the Seebeck coefficient increased and then decreased (Fig. 5b) as the hot junction temperature increased, for the PZM composites. This is an indication of semiconductor behavior. Seebeck coefficient increased linearly (Fig. 5b) for the 15% weight nano-composite, which demonstrates semi-metallic behavior. This can be attributed to the mobile charge carriers arising due to the distribution of the ZM particles in the pure polypyrrole [84]. The nano-composites have different Seebeck coefficients (Fig. 5b), for different weight percent of ZM in polypyrrole, at different temperature values. Each nanocomposite has a high Seebeck coefficient for a particular weight percent. The nanocomposites therefore obey the percolation theory [84]. The thermo power factor is directly proportional (Fig. 5c) to the d.c. conductivity for the PZM (45%) composites but is almost constant for the rest of the nanocomposites.

The thermo power factor decreases (Fig. 5d) at lower inverse hot junction temperatures and remains constant (Fig. 5d) at all other temperature ranges for the PZM composites.

3.6 a.c. conductivity study

The conductance (G) measured from 20 Hz to 1 MHz was used to calculate a.c. conductivity ($\sigma_{a.c.}$), using the following expression:

$$\sigma_{a.c.} = G \times (d/A)$$

where d is the thickness, $A = \pi r^2$ is the cross-sectional area and r is the radius of the sample pellet.

A common property for almost all the intrinsic conducting polymers such as polyaniline, polypyrrole, etc. is an extended localization in their polymer backbone. In polypyrrole, a one-dimensional chain of identical monomer units has π electrons but upon polymerization the spatial extent of these electrons is influenced by significant overlap. The electrons become delocalized over the length of the polymer chain in the form of bands and the distortion of the polymer chain around the injected charge carriers leads to formation of polarons and thereby leads to conductivity [85].

The a.c. conductivity increases with increase of frequency at the chosen temperature, for the composites. This
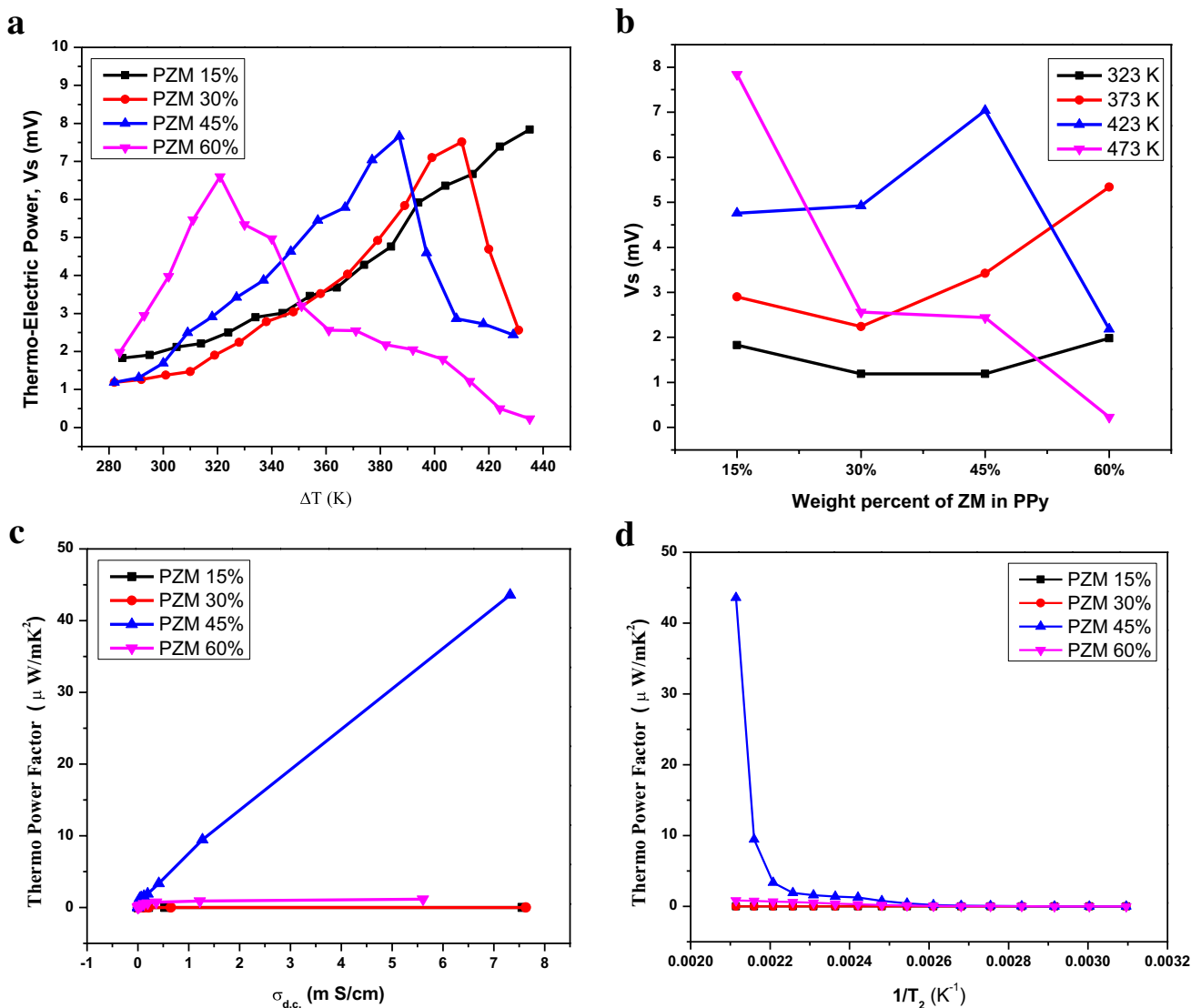
Fig. 5 **a** Thermo-electric power as a function of hot junction temperature for the PZM composites. **b** Seebeck coefficient as a function of weight percent of PZM in polypyrrole. **c** Thermo power factor as a function of d.c. conductivity for nanocomposites. **d** Thermo power factor as a function of inverse hot junction temperature for the PZM composites

phenomenon is a common respond for intrinsically conducting polymer based composites [86].

It was observed from Fig. 6a, that the a.c. conductivity increases [49] at higher frequency range and is constant at the lower frequency range, for all the composites. It was also seen that the value of conductivity (0.0385 S cm^{-1}) increases for the PZM (30 wt%) composites. This may be due to the extended chain length of polypyrrole which facilitates the hopping of charge carriers when the content of ZM is increased [85] and may also be due to the variation in the distribution of the ZM particles which supports an increased number of charge carriers to hop between favorable localized sites.

The conductivity increases for 30 wt% of ZM (Fig. 6b) in the pure PPy and decreases thereafter. This weight percent is the percolation threshold [87] for these PPy based composites. The composites obey the percolation theory. Furthermore, a decrease in the conductivity can be observed for the other composites and this can be ascribed to the distribution of ZM particles of larger grain sizes, which are partially responsible for blocking the hopping of charge carriers.

3.7 Dielectric properties studies

Dispersant/matrix interactions and the physical properties of the matrix influence the agglomeration of the dispersant

a

b
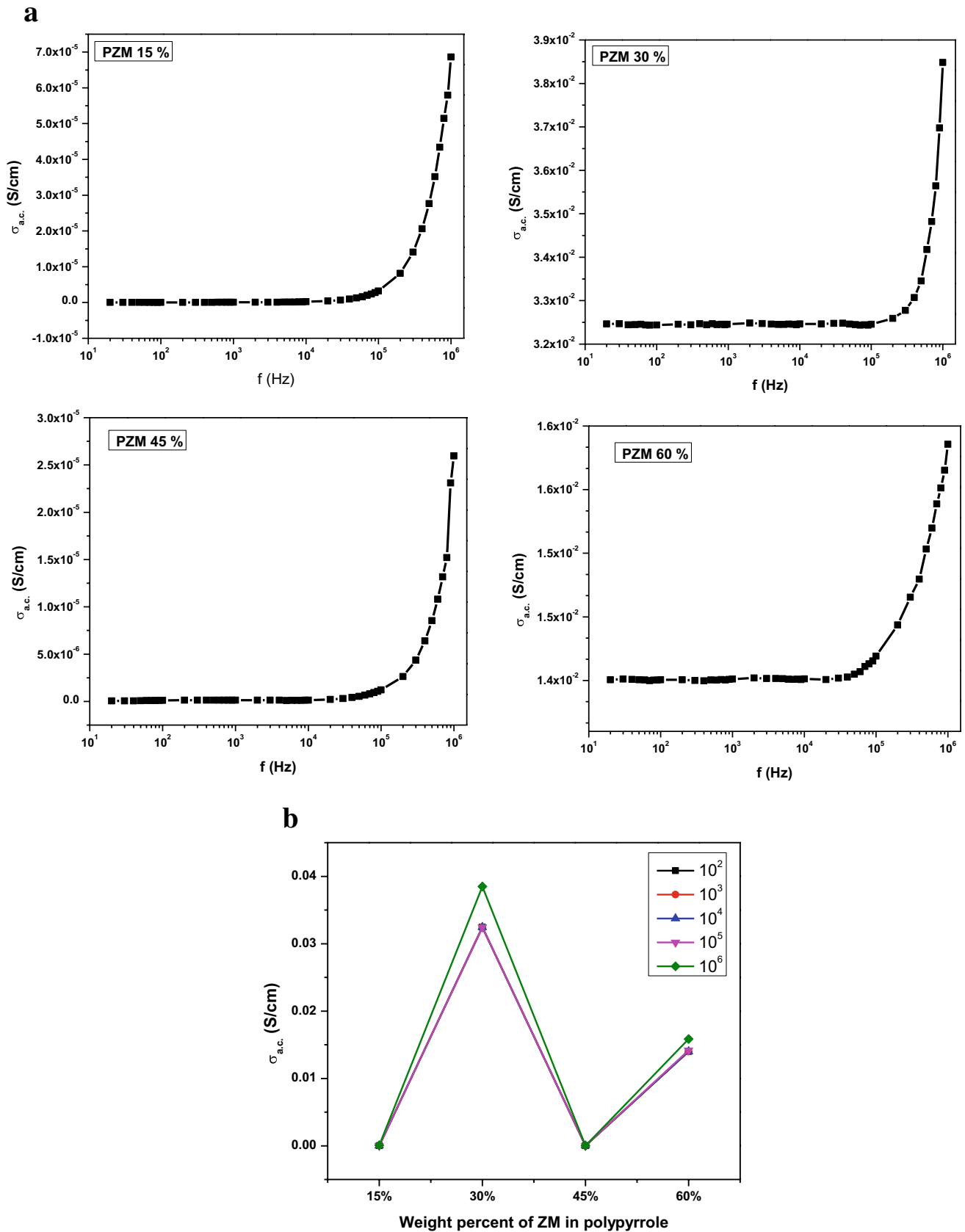
Fig. 6 **a** a.c. conductivity as a function of frequency for the PZM composites. **b** a.c. conductivity as a function of weight percent for the PZM composites

phase, which in turn, affects the dielectric properties of the composites. In case of the conducting polymers, the degree of cross-linking [88] between the polymeric chains affects the transport properties in the composites. The concentration of PZM was varied in order to investigate the influence of dopant compositions on the dielectric constant, dielectric loss and tangent loss of polypyrrole based composites.

The dielectric parameter as a function of frequency is described by the complex permittivity in the form:

$$\varepsilon^* = \varepsilon' - \varepsilon''$$

where the real part ε' and imaginary part ε'' are the components for the dielectric relative permittivity and dielectric loss respectively.

The capacitance (C) was used to calculate the dielectric constant (ε') using the following expression:

$$\varepsilon' = C \times (d/A)$$

where d is thickness and $A = \pi r^2 (r = \text{radius})$ is surface area of the nano-composite.

The measured conductance (G) was used to calculate the dielectric loss (ε'') using the following expression:

$$\varepsilon'' = G \times \left(d/\varepsilon_0 \omega A\right)$$

where angular frequency $\omega = 2\pi f$ (f = frequency) and $\varepsilon_0 =$ permittivity in free space.

The tangent loss (Tan δ) can be calculated using the following expression:

$$\text{Tan } \delta = \varepsilon''/\varepsilon'$$

The dielectric constant (Fig. 7a) decreases with increasing frequency. This may be attributed to the tendency of dipoles in the PZM composites to orient themselves in the direction of the applied electric field. However, at the high frequency range, the value remained a constant with respect to frequency. This trend was observed for all the graphs and it could be explained by the fact that higher frequencies might hinder the rotation of the dipoles thereby making it difficult for them to reorient On the other hand, the high value of ε' at low frequency might be due to the electrode and interfacial effects of the composites [89–103].

The dielectric constant increases for 30 wt% of ZM (Fig. 7b) in the pure PPy and decreases thereafter. This weight percent is the percolation threshold [89] for these PPy based composites. The composites obey percolation theory.

It is clear from Fig. 7c that, the dielectric loss (ε'') decreases with increasing frequency. The larger value of dielectric loss at low frequency could be due to the mobile charges, within the polymer backbone. On the other hand, the mobile charges (polarons) that belong to the pure PPy could be held accountable for the lower value of ε'' at high frequency [89–104].

The dielectric loss increases for 60 wt% of ZM (Fig. 7d) in the pure PPy and decreases thereafter. This weight percent is the percolation threshold [89] for these PPy based composites. The composites obey percolation theory.

The tan delta increases for 60 wt% of ZM (Fig. 7e) in the pure PPy and decreases thereafter. This weight percent is the percolation threshold [89] for these PPy based composites.

60 wt% of ZM (Fig. 7f) in the pure PPy has highest Tan delta and decreases from this point. This weight percent is the percolation threshold [70] for these PPy based composites. The composites obey percolation theory.

3.8 Dielectric electrical modulus

Dielectric constant and dielectric loss have high values at lower frequency range. ε' and ε'' deceased to nearly zero as frequency increased to higher range indicating the existence of a dielectric relaxation. This behavior may be attributed to an interfacial polarization called as Maxwell–Wanger–Sillars Effect. In order to get further information about the dielectric relaxation of the composites, ε^* has been transformed to electrical modulus M* as follows:

$$M^* = \frac{1}{\varepsilon^*} = \frac{1}{\varepsilon' - j\varepsilon''} = M' + jM''$$

where $M' = \frac{\varepsilon'}{(\varepsilon')^2 + (\varepsilon'')^2}$ and $M'' = \frac{\varepsilon''}{(\varepsilon')^2 + (\varepsilon'')^2}$, M' and M'' are real and imaginary parts of electrical modulus respectively [21, 49, 85, 86].
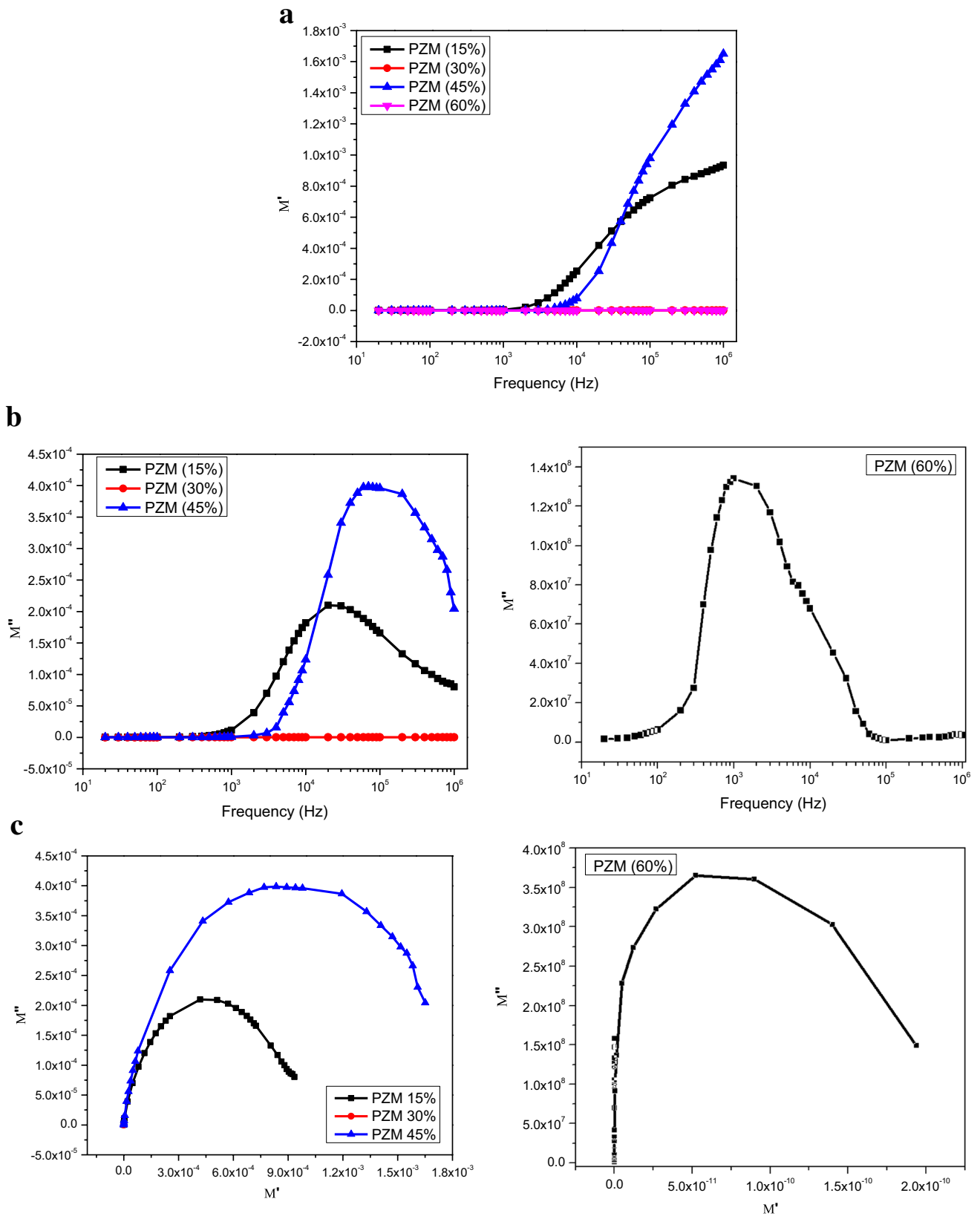
The real part of dielectric electrical modulus showed constant at lower frequency range and an increasing trend at higher frequency range (Fig. 8a) with the increase in frequency. M' is frequency independent at lower frequency range showing that the electrode (dipole) polarization makes a negligible contribution and M' is strongly frequency dependent showing very good orientation at high frequency range in the real part of electric modulus. The step-wise transition of M' at high frequency range is observed for the composites. On the frequency range of this transition, the values of M'' exhibit a peak, at a characteristic relaxation frequency f_{max}, which indicates a relaxation process. Figure 8b has shown that, the maximum of the relaxation peaks in M'' increases for PZM (45%) composite as the PZM content increases and peak is decreased for other composites [35].

Figure 8c revealed that the variation of M'' with respect to M'. It was observed from the figure that, all the PZM composites had obtained semicircular curves. As the content of PZM changes in polypyrrole, the area of the curves increases for the PPy/PZM (45%) composite since it has low conductivity and the area of the curves decreases for the PPy/PZM (30%) composite since it has high conductivity [35].
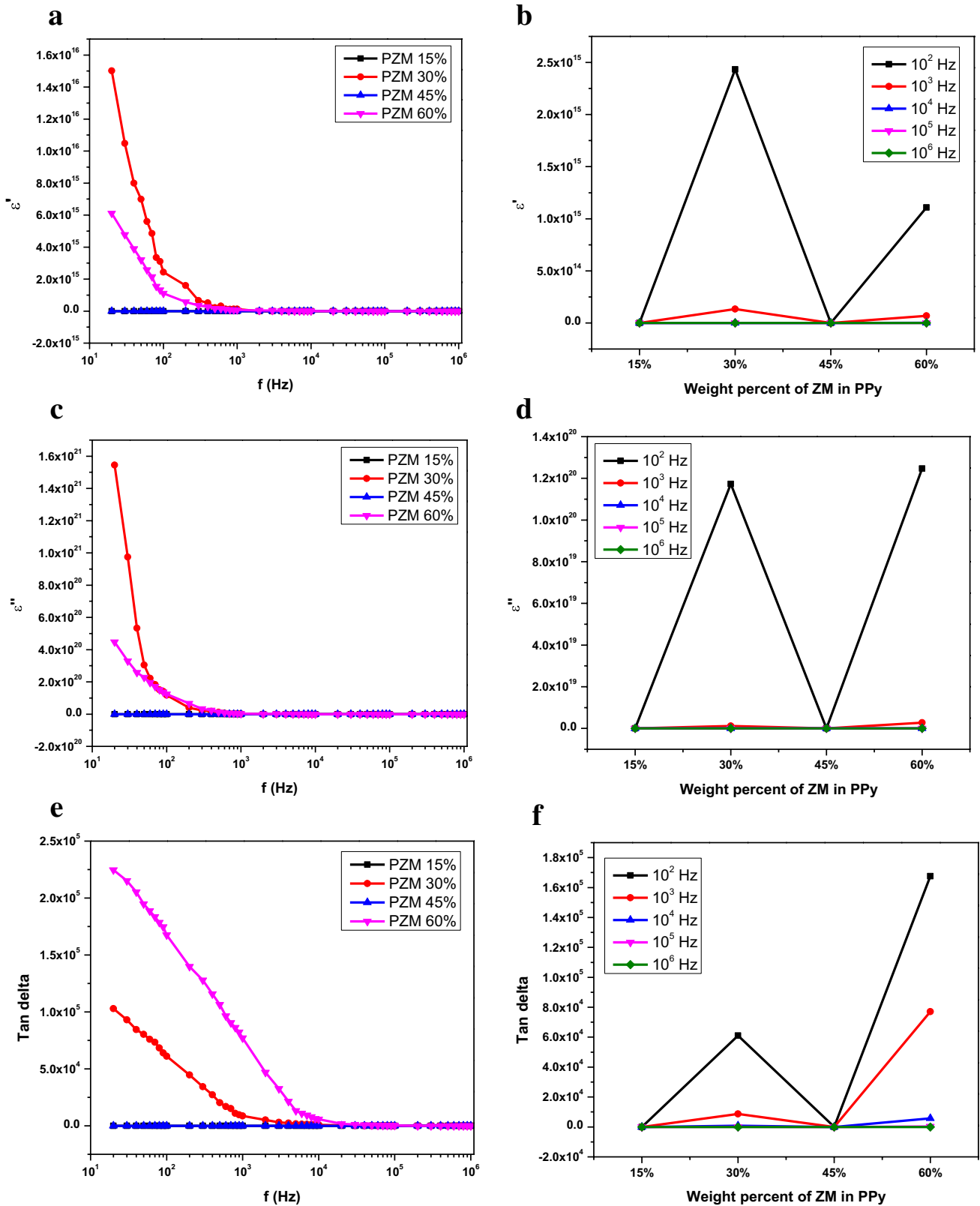
Fig. 7 a Dielectric constant as a function of frequency for the PZM composites. **b** Dielectric constant as a function of weight percent for the PZM composites. **c** Dielectric loss as a function of frequency for the PZM composites. **d** Dielectric constant as a function of weight percent for the PZM composites. **e** Tan delta as a function of frequency for the PZM composites. **f** Tan delta as a function of weight percent for the PZM composites

Fig. 8 **a** Variation of real part of electrical modulus as a function of frequency for the PZM composites. **b** Variation of imaginary part of electrical modulus as a function of frequency for the PZM composites. **c** Imaginary part versus real part of electrical modulus of the PZM composites
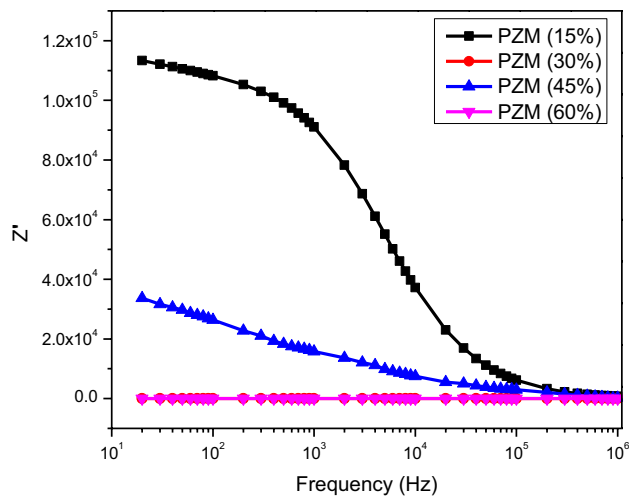
Fig. 9 Variation of real part of electrical impedance as a function of frequency for the PZM composites

3.9 Dielectric electrical impedance

Real and imaginary parts of electrical impedances were measured using following equations:

$$Z' = \frac{3.14 Z \cos \phi}{180}$$

and

$$Z'' = \frac{3.14 Z \sin \phi}{180}$$

where ϕ is phase angle and Z is impedance [49, 85, 86].

Figure 9 showed that dielectric electrical impedance decreases as frequency increases and stood constant at very higher frequency range. The polypyrrole/PZM (15%) composite has shown high value of electrical impedance.

4 Conclusion

The composites were synthesized and rigorous efforts were made to improve their transport properties. The FTIR, SEM and XRD analyses were done for the samples. The thermo electric power and transport properties studies help us conclude that there is an interaction between polypyrrole & ZM particles and that the weight percent of ZM particles also have a considerable influence on the pure polypyrrole. The composites, in general have better thermo electric factor and transport properties. Hence, the composites may be used in micro power generator and thermo cooler. The composites also might found applications in sensors i.e. gas, thermal and humidity sensors.

References

1. G. Inzelt, J. Solid State Electrochem. **15**, 1711–1718 (2011)
2. H. Shirakawa, E.J. Louis, A.G. MacDiarmid, C.K. Chiang, A.J. Heeger, J. Chem. Soc. Chem. Commun. 578–580 (1977)
3. S. Ramakrishnan, *Resonance* (Vol. 2, No. 11, 1997), pp. 48–58
4. T. Miura, R. Tao, S. Shibata, T. Umeyama, T. Tachikawa, H. Imahori, Y. Kobori, J. Am. Chem. Soc. **138**, 5879–5885 (2016)
5. K.R. Reddy, K.V. Karthik, S.B. Benaka Prasad, S.K. Soni, H.M. Jeong, A.V. Raghu, Polyhedron **120**, 169–174 (2016)
6. K.R. Reddy, K.-P. Lee, A.I. Gopalan, J. Nanosci. Nanotech. **7**, 3117–3125 (2007)
7. Y.-P. Zhang, S.-H. Lee, K.R. Reddy, A.I. Gopalan, K.-P. Le, J. Appl. Polym. Sci. **104**, 2743–2750 (2007)
8. K.R. Reddy, K.-P. Lee, A.I. Gopalan, J. Appl. Polym. Sci. **106**, 1181–1191 (2007)
9. K.R. Reddy, K.-P. Lee, A.I. Gopalan, A.M. Showkat, Polym. J. **38**, 349–354 (2006)
10. K.R. Reddy, K.-P. Lee, Y. Lee, A.I. Gopalan, J. Colloid Interface Sci. **335**, 34–39 (2009)
11. M. Hassan, K.R. Reddy, E. Haque, S.N. Faisal, S. Ghasemi, A.I. Minett, V.G. Gomes, Compos. Sci. Tech. **98**, 1–8 (2014)
12. K.K. Reddy, R.H.M. Jeong, Y. Lee, A.V. Raghu, J. Polym. Sci. Polym. Chem. Part A **48**, 1477–1484 (2010)
13. A.K. Bakhshi, Bull. Mater. Sci. **18**(5), 469–495 (1995)
14. M. Fatih Koleli, Y. Dudukcu, Arslan, Turkish J. Chem. **24**, 333–341 (2000)
15. M. Angelopoulos, IBM J. Res. Dev. **45**(1), 57–75 (2001)
16. A.J. Heeger, *Semiconducting and Metallic Polymers: The Fourth Generation of Polymeric Materials, Nobel Lecture*, 8th (2000)
17. T.P. Radhakrishnan, Resonance, 62–70 (2001)
18. T.V. Vernitskaya, O.N. Efimov, Russ. Chem. Rev. **66**(5), 443–457 (1997)
19. E. Buhks, I.M. Hodge, J. Chem. Phys. **83**(11), 5976–5980 (1985)
20. T.A. Skotheim ed. *Handbook of Conducting Polymers, Vols. 1–2,*. (Marcel Dekker, New York, 1986)
21. K.C. Sajjan, A.S. Roy, A. Parveen, S. Khasim, J. Mater. Sci.: Mater. Electron. **25**, 1237–1243 (2014)
22. T. Machappa, M.V.N. Ambika Prasad, Bull. Mater. Sci. **35**(1), 75–81 (2012)
23. N. Parvathikar, S. Jain, S. Khasim, M. Revansiddappa, S.V. Bhoraskar, M.V.N. Ambika Prasad, Sens. Actuators. B **114**, 599–603 (2006)
24. B.V. Chaluvaraju, S.K. Ganiger, M.V. Murugendrappa, I.J. Resea. Pure Appl. Phys. **5**(1), 13–18 (2015)
25. I.A. Salem, R.I. Elhag, K.M.S. Khalil, Trans. Met. Chem. **25**, 260–264 (2000)
26. A. Afzal, Mater. Express. **4**(1), 1–12 (2014)
27. B.V. Chaluvaraju, S.K. Ganiger, M.V. Murugendrappa, Polym. Sci. Ser. B **56**(6), 935–939 (2014)
28. F.F. Ferreira, T.G.S. Cruz, M.C.A. Fantini, M.H. Tabacniks, S.C. de Castro, J. Morais, A. de Siervo, R. Landers, Solid State Ionics **357**, 136 (2000)

29. C. Zollfrank, K. Gutbrod, P. Wechsler, J.P. Guggenbichler, Mater. Sci. Eng. C **32**, 47 (2012)
30. B.V. Chaluvaraju, S K. Ganiger, M.V. Murugendrappa. Polym. Sci. Ser. B **56**(6), 935–939 (2014)
31. B.V. Chaluvaraju, S.K. Ganiger, M.V. Murugendrappa, IJLTEMAS, **III**(V), 33–36 (2014)
32. H. Wang, L. Wang, R. Wang, X. Tian, K. Zheng, Colloid. Polym. Sci. **291**, 1001–1007 (2013)
33. C. Basavaraja, Y. Veeranagouda, K. Lee, T.K. Vishnuvardhan, R. Pierson, D.S. Huh, J. Polym. Res. **17**, 233–239 (2010)
34. S.K. Ganiger, B.V. Chaluvaraju, M.V. Murugendrappa, International JIRSET, **4**(7), 5819–5827 (2015)
35. B.V. Chaluvaraju, U.P. Raghavendra, T.S. Pranesha, M.V. Murugendrappa, J. Mater. Sci.: Mater. Electron. **28**, 11230–11242 (2017)
36. D.M. Jundale, S.T. Navale, G.D. Khuspe, D.S. Dalavi, P.S. Patil, V.B. Patil, J. Mater. Sci.: Mater. Electron. **24**, 3526–3535 (2013)
37. D.S. Madddison, J. Unsworth, Synth. Metals. **26**, 99–108 (1988)
38. C. Han, Z. Li, S. Dou, Chin. Sci. Bull. **59**(18), 2073–2091 (2014)
39. L.E. Bell, Science **321**, 1457–1461 (2008)
40. A. Shakouri, M. Zebarjadi, S. Volz eds. *Thermal Nanosystems and Nanomaterials*, (Springer, Heidelberg, 2009)
41. D. Kraemer, B. Poudel, H.P. Feng, Nat. Mater. **10**, 532–538 (2011)
42. A.F. Ioffe, *Physics of Semiconductors*. (Academic Press, New York, 1960)
43. A. Majumdar, Science **303**, 777–778 (2004)
44. P. Pichanusakorn Bandaru, Mater. Sci. Eng. **67**, 19–63 (2010)
45. A. Shakouri, Ann. Rev. Mater. Res. **41**, 399–431 (2011)
46. N. Dubey, M. Leclerc, J. Polym. Sci. B: Polym. Phys. **49**, 467–475 (2011)
47. J.L. Njoroge, Mater. Res. Bull. **35**, 909–910 (2010)
48. M. He, F. Qiu, Z.Q. Lin, Energy Environ. Sci. **6**, 1352–1361 (2013)
49. J. Harreld, H.P. Wong, B.C. Dave, B. Dunn, L.F. Nazar, J. Non-Cryst. Solids. **225**, 319–324 (1998)
50. S. Kazim, S. Ahmad, J. Pfleger, J. Plestil, Y.M. Joshi, J. Mater. Sci. **47**, 420–428 (2012)
51. M.V. Murugendrappa, M.V.N. Ambika Prasad, J. Appl. Polym. Sci. **103**, 2797–2801 (2007)
52. V.S. Reddy Channu, R. Holze, Ionics **18**, 495–500 (2012)
53. S. Sarmah, A. Kumar, Indian J. Phys. **85**(5), 713–726 (2011)
54. M. Dahlhaus, F. Beck, J. Appl. Electrochem. **23**, 957–965 (1993)
55. Z. Huang, S. Wang, H. Li, S. Zhang, Z. Tan, J. Therm. Anal. Calorim. **115**, 259–266 (2014)
56. A. Rherari, M. Addou, M. Haris, J. Mater. Sci.: Mater. Electron. **28**(21), 15762–15767 (2017)
57. V. Jadkar, A. Pawbake, R. Waykar, A. Jadhavar, J. Mater. Sci.: Mater. Electron. **28**(21), 15790–15796 (2017)
58. W.B. Soltan, M.S. Lassoued, S. Ammar, T. Toupance, J. Mater. Sci.: Mater. Electron. **28**(21), 15826–15834 (2017)
59. P.L. Deepti, S.K. Patri, R.N.P. Choudhary, J. Mater. Sci.: Mater. Electron. **28**(21), 16071–16076 (2017)
60. J. Hou, G. Zhu, J. Zheng, Polym. Sci.: Ser. B **53**(9–10), 546–552 (2011)
61. Z. Shen, D. Li, J. Mater. Sci.: Mater. Electron. **28**(18), 13257–13266 (2017)
62. M. Jose, M. Elakiya, S.A. Martin Britto Dhas, J. Mater. Sci.: Mater. Electron. **28**(18), 13649–13658 (2017)
63. B.V. Chaluvaraju, K. Sangappa, S.K. Ganiger, M.V. Murugendrappa, Polym. Sci.: Ser. B **56**(6), 935–939 (2014)
64. O.G. Abdullah, R.R. Hanna, Y.A.K. Salman, J. Mater. Sci.: Mater. Electron. **28**(14), 10283–10294 (2017)
65. Y. Suiyan Ma, L.X. Shi, M. Zhao, D. Liu, J. Mater. Sci.: Mater. Electron. **28**(21), 15154–15160 (2017)
66. B.K. Das, T. Das, K. Parashar, A. Thirumurugan, S.K.S. Parashar, J. Mater. Sci.: Mater. Electron. **28**(20), 15127–15134 (2017)
67. B. Singh, A. Thakur, M. Kumar, S.K. Verma, D. Jasrotia, J. Mater. Sci.: Mater. Electron. **28**(14), 10007–10011 (2017)
68. Y. Yuan, Y. Qian, H. Han, Y. Chen, J. Mater. Sci.: Mater. Electron. **28**(14), 10028–10034 (2017)
69. B. Mohanbabu, R. Bharathikannan, G. Siva, J. Mater. Sci.: Mater. Electron. **28**(18), 13740–13749 (2017)
70. K. Mohammadi, M. Sadeghi, R. Azimirad, J. Mater. Sci.: Mater. Electron. **28**(14), 10042–10047 (2017)
71. F. Namvar, F. Beshkar, M. Salavati-Niasari, S. Bagheri, J. Mater. Sci.: Mater. Electron. **28**(14), 10313–10320 (2017)
72. Y.Y. Wang, K.F. Cai, J.L. Yin, B.J. An, Y. Du, X. Yao, J. Nanoparticle Res. **13**, 533–539 (2011)
73. Q. Tang, X. Sun, Q. Li, J. Lin, J. Wu, J. Mater. Sci. **44**, 849–854 (2009)
74. T.J. Kang, S. Miyata, Y. Miyaki, Polym. Bull. **31**, 593–599 (1993)
75. J.H. Chen, Z.P. Huang, D.Z. Wang, S.X. Yang, J.G. Wen, Z.F. Ren, Appl. Phys. A **73**, 129–131 (2001)
76. H. Eisazadeh, World J. Chem. **2**(2), 67–74 (2007)
77. M.P. Dash, P.L. Nayak, Int. J. Plast. Tech. **14**(2), 142–151 (2010)
78. R. Turcu, M. Brie, G. Leising, V. Tosa, A. Mihut, A. Niko, A. Bot, Appl. Phys. A **67**, 283–287 (1998)
79. S. Geetha, D.C. Trivedi, J. Mater. Sci.: Mater. Electron. **16**,, 329–333 (2005)
80. M.M. Abdia, H.N.M. Ekramul Mahmudb, A. Kassima, W.M.M. Yunusc, Z.A. Talibc, M.J. Harona, Polym. Sci. **52**(11–12), 662–669 (2010)
81. H.-R. Yin, J.-S. Jiang, J. Mater. Sci. **40**, 3013–3015 (2005)
82. N. Srivastava, Y. Singh, R.A. Singh, Bull. Mater. Sci. **34**(4), 635–638 (2011)
83. A. Skotheim, J.R. Reynolds, *Conjugated Polymers: Theory, Synthesis, Properties and Characterization, Handbook of Conducting Polymers*, 3rd edn (CRC Press, Taylor and Francis Group, Boca Raton, 2007)
84. T. Dhandayuthapani, R. Sivakumar, R. Ilangovan, J. Mater. Sci. **28**(20), 15074–15080 (2017)
85. B.V. Chaluvaraju, S.K. Ganiger, M.V. Murugendrappa, Polym. Sci. **57**(4), 467–472 (2015)
86. T. Uma, H.Y. Tu, S. Warth, D. Schneider, D. Freude, U. Stimming, J. Mater. Sci. **40**, 2059–2063 (2005)
87. S.K. Ganiger, B.V. Chaluvaraju, K.S. Ganiger, M.V. Murugendrappa, Malays. Polym. J. **10**(1), 9–15 (2015)
88. P. Dutta, S. Biswas, M. Ghosh, S.K. De, S. Chatterjee, Synth. Met. **122**, 455–461 (2000)
89. H.P. de Oliveira, M.V.B. dos Santos, C.G. dos Santos, C.P. de Melo, Synth. Met. **135–136**, 447–448 (2003)
90. H. Narayan, A.M. Montano, M.L. Hernandez, J.A. Hernandez, C.P. Gonzalez, C.A. Ortiz, J. Mater. Environ. Sci. **3**(1), 137–148 (2012)
91. T.K. Vishnuvardhan, V.R. Kulkarni, C. Basavaraja, S.C. Raghavendra, Bull. Mater. Sci. **29**(1), 77–83 (2006)
92. N. Kumar, N. Bastola, S. Kumar, R. Ranjan, J. Mater. Sci. **28**(14), 10420–10426 (2017)
93. S. Bhavani, M. Ravi, Y. Pavani, V. Raja, R.S. Karthikeya, V.V.R.N. Rao, J. Mater. Sci. **28**(18), 13344–13349 (2017)
94. Q. Chi, Z. Gao, C. Zhang, Y. Cui, J. Mater. Sci. **28**(20), 15142–15148 (2017)
95. K. Prompa, E. Swatsitang, T. Putjuso, J. Mater. Sci. **28**(20), 15033–15042 (2017)
96. S. Halder, K. Parida, S.N. Das, S. Bhuyan, R.N.P. Choudhary, J. Mater. Sci. **28**(21), 631–637 (2017)
97. K. Sangappa, B. Ganiger, V. Chaluvaraju, M.V. Murugendrappa, IJIRSET **3**(6), 13934–13946 (2014)

98. Y.D. Kim, G.G. Hong, Korean J. Chem. Eng. **29**(7), 964–968 (2012)
99. T.Z. Abdul Shakoor, M. Rizvi, Saeed, Polym. Sci. **54**(5), 401–406 (2012)
100. Y.D. Kim, J.H. Kim, Colloidal Polym. Sci. **286**, 631–637 (2008)
101. M.H. Harun, E. Saion, A. Kassim, E. Mahmud, M.Y. Hussain, I.S. Mustafa, J. Adv. Sci. Arts **1**, 9–16 (2009)
102. P. Tsotra, K. Friedrich, J. Mater. Sci. **40**, 4415–4421 (2005)
103. M. Lakshmi, A. Roy, S. Khasim, M. Faisal, K.C. Sajjan, M. Revanasiddappa, AIP Adv. **3**, 112113–112118 (2013)
104. V.B. Aaditya, B.M. Bharatesh, R. Harshitha, B.V. Chaluvaraju, U.P. Raghavendra, M.V. Murugendrappa, J. Mater. Sci. (2017). https://doi.org/10.1007/s10854-017-8214-6